Oxygen Evolution Reaction

International Edition: DOI: 10.1002/anie.201902884
German Edition: DOI: 10.1002/ange.201902884

Oxygen Evolution Reaction at Carbon Edge Sites: Investigation of Activity Evolution and Structure–Function Relationships with Polycyclic Aromatic Hydrocarbons

*Yangming Lin, Qing Lu, Feihong Song, Linhui Yu, Anna K. Mechler, Robert Schlögl, and Saskia Heumann**

Abstract: *The abundance of available surface chemical information and edge structures of carbon materials have attracted tremendous interest in catalysis. For the oxygen evolution reaction (OER), the edge effects of carbon materials have rarely been studied in detail because of the complexity of various coexisting edge configurations and the controversy between carbon corrosion and carbon catalysis. Herein, the exact roles of common carbon active edge sites in the OER were interrogated using polycyclic aromatic hydrocarbons (PAHs) with designated configurations (zigzag and armchair) as model probe molecules, with a focus on structure–function relationships. Zigzag configurations of PAHs showed high activity for the OER while also showing a good stability at a reasonable potential. They show a TOF value of 0.276 s^{-1} in 0.1 M KOH. The catalytic activity of carbon edge sites was further effectively regulated by extending the π conjugation structure at a molecular level.*

The oxygen evolution reaction (OER) has attracted considerable interest due to its significance in obtaining hydrogen by the electrochemical splitting of water.[1] In contrast to the common metal-based catalysts, carbocatalysts can be produced at low cost and are sustainable. It has been shown recently that metal-free carbon-based electrocatalysts are compelling alternatives for improving the activity and durability of the OER.[2] It should be mentioned that, as a consequence of the extremely complex surface structure (e.g. coexistence of various kinds of foreign groups and edges species) of carbocatalysts, some important issues with regard to the OER mechanism still remain unclear to date.[3] For example, a perfect graphitic carbon material is less competitive for the OER, but the presence of dopants or active edge sites (heteroatom-free) leads to promising reactivity since they can change the electronic structures of the carbon network.[4] Among them, zigzag and armchair configurations are the most common structural edge geometries, which have unique electronic properties compared with the basal plane of graphitic structures and thus exhibit some distinctive chemical behaviors in catalysis.[5] However, the detailed functions of those two carbon active edge configurations for the activation of water molecules have so far rarely been studied. Therefore, an effective approach to understand the roles of edge configurations in the catalysis of the OER is of critical importance for elaborating both metal-free and heteroatom-free carbon materials (without nitrogen or oxygen species).

Actually, there is a common view that it is very difficult to identify the specific structures and roles of the carbon edge sites experimentally since a wide range of edge species coexist in carbon materials. Compared to carbon materials, polycyclic aromatic hydrocarbons (PAHs) are a class of unique compounds that consist of fused conjugated aromatic rings and do not contain heteroatoms or carry substituents.[6] Various PAHs with a single edge configuration could be selectively designed (Scheme 1 a). Moreover, PAHs have a similar carbon network structure, surface properties, and an electronic conjugated π system that can be tuned by extending the benzene units. They can be used directly as model probe molecules to mimic the armchair and zigzag edge structures of carbocatalysts and to probe the specific activation process for catalysis.[7] However, the low electric conductivity and the poor electron transfer property of PAHs hamper their sole applications in electrochemical reactions. A nondestructive

[*] Dr. Y. M. Lin, Dr. Q. Lu, F. Song, Dr. L. Yu, Dr. A. K. Mechler, Prof. Dr. R. Schlögl, Dr. S. Heumann
Max Planck Institute for Chemical Energy Conversion
Stiftstrasse 34–36, Mülheim an der Ruhr, 45470 (Germany)
E-mail: saskia.heumann@cec.mpg.de
Prof. Dr. R. Schlögl
Department of Inorganic Chemistry
Fritz Haber Institute of the Max Planck Society
Faradayweg 4–6, Berlin, 14195 (Germany)
Supporting information and the ORCID identification number for one of the authors of this article can be found under: https://doi.org/10.1002/anie.201902884.

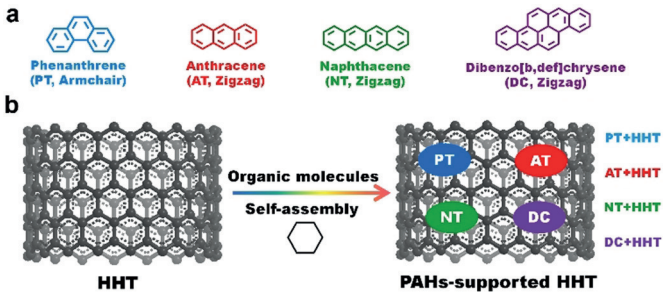

Scheme 1. a) Edge structures of four kinds of PAHs with designated configurations. b) The schematic process of generating PAH + HHT by a self-assembly method.

solution based on strong π–π interactions with nanocarbons as supports has recently been proposed.[8] The obtained catalysts exhibit promising applications in the OER.

Herein, we used two typical carbon materials as supports: HHT, a commercial carbon nanofiber treated at a high temperature of 3000 °C that has a well-graphitized structure, extremely low defect ratio ($I_D/I_G = 0.34$), high conductivity (15 S cm^{-1}), and a surface area of 34 m^2 g^{-1} (see Figure S2 in the Supporting Information),[5] and OLC, an onion-like carbon nanodiamond which was annealed at 1500 °C and has a high surface area (460 m^2 g^{-1}; see Figure S3).[9] To engineer the composite materials, highly dispersed PAH model molecules with the desired zigzag (anthracene (AT), naphthacene (NT), dibenzo[*b*,*def*]chrysene (DC)) or armchair (phenanthrene, PT) configurations were deposited on the support materials by a self-assembly method (see Scheme 1b and Scheme S1). As a reference, T-HHT was obtained by the same process but without the introduction of one of the model molecules. The obtained monosupported carbon materials have a reasonable concentration of the desired edge configurations and allow an experimental investigation of the intrinsic activities of typical carbon edge configurations for the OER. The carbon materials exhibited an enhanced activity for splitting water. The reactivities of the supported catalysts in 0.1 M KOH mainly originate from carbocatalysis rather than carbon corrosion. The zigzag configuration was determined to have a more positive influence than the armchair edge sites on the OER.

Figure 1a shows thermogravimetric (TG) measurements of PT + HHT and AT + HHT; the onset temperatures are clearly increased to 152 °C and 225 °C, respectively, compared to the 110 °C for pure PT and 185 °C for pure AT. This finding indicates that there might be a strong π–π interaction between the deposited molecules and the HHT support. The net content of PT + HHT and AT + HHT samples was calculated by the difference in the mass loss compared to that of pure HHT, which resulted in about 0.53 wt% and 0.60 wt%, respectively. The infrared (IR) spectra recorded in the attenuated total reflectance (ATR) mode show that the molecular structures of AT and PT remain unaffected and are not destroyed during the preparation process (Figures S4 and S5). The OER activities of both kinds of organic molecules and their corresponding catalysts when supported on HHT were evaluated (Figure 1b). PT + HHT affords a slightly enhanced current density compared to the T-HHT reference sample. Its E_{onset} value is close to 1.57 V versus RHE. In contrast, the AT + HHT catalyst shows the smallest onset potential (E_{onset}) of 1.54 V versus RHE and achieves a current density of 0.45 mA cm^{-2} at 1.6 V. As a reference, pure AT and PT molecules do not generate an elevated current density. To assess their intrinsic catalytic abilities, the theoretical turnover frequency (TOF) of representative AT + HHT and PT + HHT catalysts at 1.6 V were also calculated (inset of Figure 1b, based on the mass results of TG). The AT + HHT catalyst shows a good TOF value of about 0.113 s^{-1}, much higher than that of the PT + HHT catalyst (0.022 s^{-1}). The TOF is significantly higher than those of reported highly active OER catalysts.[10] The corresponding TOF values of AT + HHT and PT + HHT calculated per carbon atom and

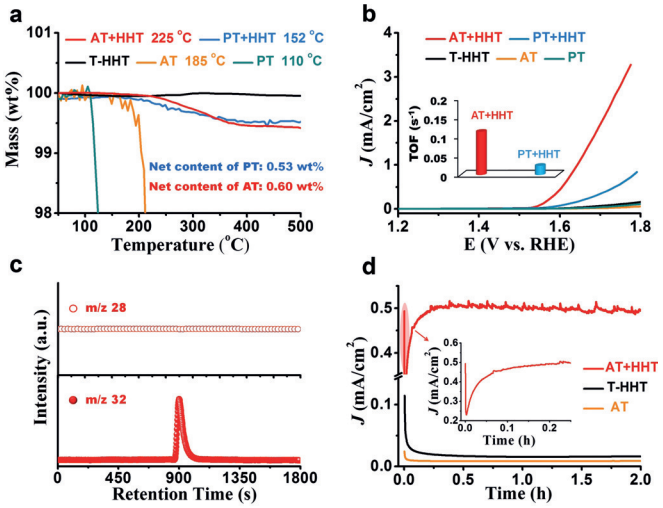

Figure 1. a) TG data of T-HHT, PT + HHT, AT + HHT, pure PT, and AT. The net contents of PT and AT molecules on the HHT catalyst were calculated from the mass loss of the PT + HHT or AT + HHT minus the mass loss of pure HHT. b) Linear sweep voltammetry (LSV) curves of various catalysts measured in argon-saturated 0.1 M KOH with a scan rate of 5 mV^{-1} with iR compensation. The inset represents the theoretical TOF values of PT + HHT and AT + HHT catalysts at 1.6 V versus RHE. All the samples were loaded at 0.051 mg cm^{-2} on the electrode. The onset potential is defined as the potential at which the corresponding current density is 0.03 mA cm^{-2}. c) Mass spectra of CO (*m*/*z* 28) and O_2 (*m*/*z* 32) of AT + HHT collected after 12 h at a constant potential of 1.6 V versus RHE. In this measurement, the loading of sample on the electrode was 0.5 mg cm^{-2}. Detailed information can be found in the Supporting Information. d) Long-term stability tests of representative AT + HHT, T-HHT, and pure AT at 1.6 V versus RHE. The inset shows the enlarged induction period of the AT + HHT catalyst.

per outer carbon atom are 0.00807 s^{-1}, 0.01883 s^{-1} and 0.00157 s^{-1}, 0.00367 s^{-1}, respectively (Figure S6). Moreover, the Tafel slope of AT + HHT (Figure S7; 71 mV dec^{-1}) is much lower than that of PT + HHT (114 mV dec^{-1}), PT (211 mV dec^{-1}), AT (214 mV dec^{-1}), and T-HHT (201 mV dec^{-1}) catalysts, thus indicating its favorable scaling of kinetics with overpotential. All these results show clearly that AT with a zigzag edge configuration plays a more positive role in the OER. The results from electrochemical impedance spectroscopy (EIS; Figure S8) imply a better charge transfer at the electrode/electrolyte interface of AT + HHT because of its smaller semicircle diameter compared with T-HHT and AT. By employing the rotating ring-disk electrode (RRDE) technique (Figure S9), the OER process occurring on AT + HHT was confirmed to be dominated by a desirable four-electron pathway (99.9%) with negligible formation of peroxide intermediates and a high Faradaic efficiency (FE(O_2)) of 90.2% at 1.6 V. These values are comparable to reported metal-based catalysts.[11] It should be emphasized that no CO signal could be observed, whereas an O_2 signal was found in the mass spectra (Figure 1c). These results further reflect the fact that the current density of the supported HHT samples mainly originates from water oxidation rather than from carbon corrosion. The loss of FE(O_2) may partly arise from the recombination of H_2 from

the counter electrode and O_2 from the working electrode. Furthermore, the inefficient oxygen collection by the Pt ring electrode or unavoidable carbon corrosion (e.g. CO_2 formation)[12] in an alkaline medium might also be reasons for faradaic losses.

The structural stability of the catalyst during the OER was investigated in a long-time test at a reasonable potential of 1.6 V versus RHE. As displayed in Figure 1 d, the current densities of T-HHT and pure AT are very low, but they are very stable for two hours. After an induction period, the observed currents of T-HHT and pure AT remain constant, which indicates their inertness, and this is further supported by the unchanged CV spectra recorded before and after the OER (Figure S10). In contrast, AT + HHT shows a specific uphill induction period, which indicates that the zigzag configuration as an active edge would undergo a pre-activation process, that is, potentially a structural transformation. Moreover, the new CV peaks located at about 0.4 V were observed after two hours testing, thus suggesting the in situ formation of specific active oxygen species during the OER, for example, phenolic species, which might facilitate the OER process.

Naphthacene (NT) and dibenzo[*b*,*def*]chrysene (DC) were then introduced as active probes with extended zigzag domains and conjugated structures to further study the structure–function relationships between zigzag edge sites and the OER activity. The net contents of NT and DC are 0.9 wt % and 1.1 wt %, respectively, by TG, as displayed in Figure S11. The ATR-IR spectra of the prepared catalysts confirm the presence of the molecular structures of NT and DC on the support (Figures S12 and S13). The LSV curves in Figure 2 a show the NT + HHT has a better activity than AT + HHT. The addition of DC, with its increased number of benzene units, results in a further improvement of the OER activity. All these PAH-supported HHT catalysts have similar Tafel slope values that range from 66 to 71 mV dec^{-1}, thus demonstrating that they exhibit the same reaction kinetics during the OER (Figure S14). Increasing the number of zigzag motifs results in a small down-shift of the E_{onset} value from 1.54 V for the AT + HHT to 1.53 V for the NT + HHT and then to 1.52 V for the DC + HHT being observed. The latter two catalysts deliver good FE(O_2) outputs of 85.5 %–90.7 % at 1.6 V (Figure S15). Moreover, as displayed in Figure 2 b, the theoretical TOF values can be improved to 0.197 s^{-1} with NT + HHT and even further to 0.276 s^{-1} with DC + HHT. These TOF values are comparable to reported metal-based heterogeneous catalysts (Table S1). A positive relationship between the current density ($J_{\Delta ECSA}$, based on the ECSA; Figures S16–S19 and 2 b) and the benzene units of the PAHs is also observed.

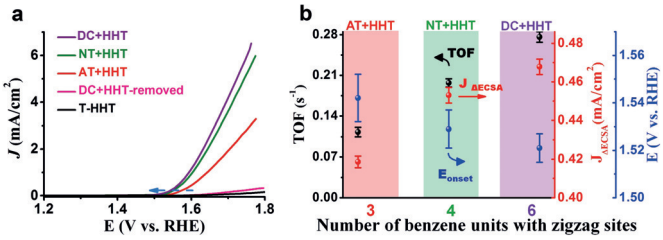

Figure 2. Electrochemical measurements of various PAH + HHT catalysts for the OER. a) LSV curves of AT + HHT, NT + HHT, DC + HHT, and removed DC + HHT. b) Number of benzene units with zigzag sites in the PAHs as a function of the theoretical TOF, E_{onset}, and electrochemically active surface area (ΔECSA) at 1.6 V versus RHE. Here, $\Delta ECSA = ECSA_{(supported\ HHT)} - ECSA_{(T\text{-}HHT)}$; detailed information on the calculation can be found in the Supporting Information. The onset potential is defined as the potential at which the corresponding current density is 0.03 mA cm^{-2}. The loadings of all the samples on the electrode were 0.051 mg cm^{-2}.

In an additional experiment, the DC molecules were removed from the HHT surface. The obtained catalyst (DC + HHT-removed) performs comparably to T-HHT, as shown by the starting values (Figure 2 a). All these facts indicate that 1) the zigzag configuration is active in the OER; 2) structures with increased π-conjugation are advantageous for the OER, and 3) the intrinsic catalytic activities of zigzag sites are associated with the sizes of exposed edge domains. It might be that PAH molecules with more benzene units have a stronger interaction with the supports and, therefore, have a better electric conductivity. It can be expected that finding a facile strategy for preparing PAH molecules with larger conjugated systems and tunable edge configurations will lead to highly active carbon-based electrodes. Research in this area is in high demand for understanding carbocatalysis and for the development of carbocatalysts with impressive performances.

We used an onion-like carbon (OLC) as an additional support to study the range of the procedure. As summarized in Figure S20, a similar performance enhancement is also successfully demonstrated with the as-prepared AT + OLC catalyst with a 2.61 wt % net content of AT (Figure S21), which outperforms PT + OLC and T-OLC samples in terms of activity. Its E_{onset} value (1.54 V) and the Tafel slope (77 mV dec^{-1}) are similar to those of the AT + HHT catalyst, which suggests they have the same active centers and reactivity kinetics in the OER. The introduction of AT also improves the ECSA of OLC from 5.89 cm^2 to 9.36 cm^2 (Figure S22). All the above results support the fact that PAHs can be used as model probes to investigate the explicit roles of edge configurations in the OER at a molecular level.

The kinetic isotope effect (KIE) is an effective experimental technique to study chemical reactions involving protons.[13] As displayed in Figure 3 a, the OER activity decreases significantly when the OER is operated in a KOH/D_2O medium. The Tafel slopes also increase from 66 mV dec^{-1} in protic solution to 81 mV dec^{-1} in deuterated solution (Figure 3 b), which indicates there is a difference in the Gibbs free energy of the intermediate that affects the reaction rate.[14] The KIE values are associated with the current density ratios in the H_2O and D_2O solutions according to: $KIE = k_H/k_D = j_0^H C_0^D / j_0^D C_0^H$ (detailed information can be found in the experimental section of the Supporting Information).[15] In the current study, the k_H/k_D value is 2.40 at 1.60 V, which suggests a significant primary isotope effect arising from a water oxidation reaction. In general, the high KIE value indicates that the rate-determining step (RDS) of the water oxidation involves a cleavage of the O–H bonds. It therefore allows us to deduce that the introduced deuterated water most likely influences the formation of active oxygen

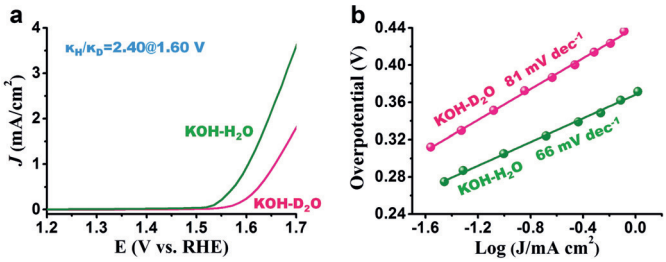

Figure 3. Electrochemical isotopic studies of representative NT + HHT catalysts. a) LSV curves of the catalyst in 0.1 M KOH dissolved in H_2O and D_2O (99.9%). b) Tafel slopes of the catalysts in KOH/H_2O and KOH/D_2O.

species *O by the deprotonation of *OD or hinder the formation of O_2 from the deoxygenation/deprotonation of active oxygen species *OOD (that is, O–O bond formation for O_2 production). Moreover, the Tafel slope at around 60 mV dec^{-1} has been considered to be a plausible indicator of a RDS involving the deoxygenation/deprotonation of the active oxygen species *OOH through a single-site mechanism.[16] As mentioned above, the Tafel slopes of NT + HHT is 66 mV dec^{-1} (Figure 2c). Therefore, it seems likely that the evolution of active *OOH species may be a RDS in the OER.

Density functional theory (DFT) calculations were performed to gain a deeper molecular-level understanding of the possible pre-activation and OER processes involving the NT model molecule. As shown in Figure 4, a zigzag configuration would be easily pre-activated by a two-step approach to produce active phenolic species that can accelerate the OER process. This proposal is consistent with the results of the edge activity, structural evolutions, and CV spectra (Figures 1d and S10). The involved active radicals occur most probably at the β-C position because of its lower energy relative to that of the α-C or γ-C locations of the zigzag structure (Figure S23). In general, the OER mechanism mainly involves *OH, *O, and *OOH intermediates. Of the possible mechanisms, the corresponding adsorption energy for the deoxygenation of the active oxygen species *OOH to produce O_2 (Figure 4, step 3) is the highest (0.6 eV), meaning that it plays the most positive role in the OER process. The relatively low

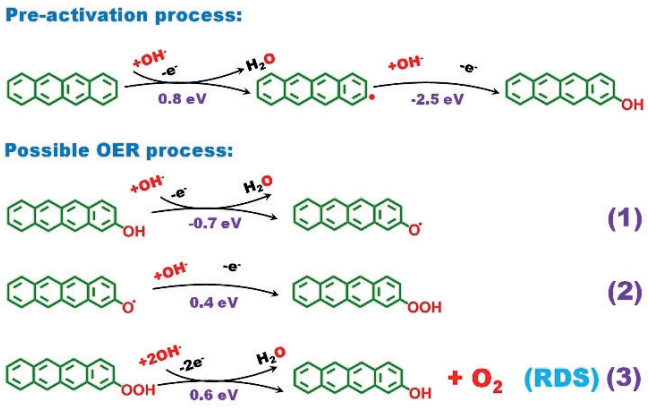

Figure 4. DFT calculations on possible pre-activation and OER processes of active NT probe molecules.

adsorption energy for the formation of the active oxygen species *O during the deprotonation process of *OH (−0.7 eV, step 1) implies that this step is not critical. In combination with the experimental isotopic electrochemical studies, we could conclude that the RDS in carbon electrocatalysts is most likely step 3, where O_2 is formed.

In summary, we have developed a facile molecular-level strategy to elucidate the explicit roles of common carbon edge sites (heteroatom-free) in the electrochemical oxygen evolution reaction (OER). Studies of polycyclic aromatic hydrocarbons (PAHs) with designated edge species as active model probes show that both armchair and zigzag motifs in nanocarbon materials play positive roles in the OER. The introduction of PAHs with zigzag configurations endows nanocarbon support materials (HHT and OLC as supports) with better performances for the OER than armchair motifs. The intrinsic catalytic activities of edge sites are coupled with the exposed domains, as demonstrated by extended π-conjugated structures. The in situ formation of phenolic oxygen species originating from structural evolution of the active edges might be responsible for accelerating the OER. The formation of O_2 from the deoxygenation of the active oxygen species *OOH is a possible rate-determining step, as illustrated by H/D kinetic isotope effects and theoretical calculations. This work offers direct evidence for understanding the roles of carbon edge sites in carbon-based metal-free catalysis.

Acknowledgements

We thank Dr. Huiqing Song and Dr. Ioannis Spanos for their kind help in MS and ICP measurements. We also thank Dongyoon Shin for the introduction to RRDE measurements. We would like to thank the Max Planck society for funding.

Conflict of interest

The authors declare no conflict of interest.

Keywords: carbon materials · edge sites · isotope effect · OER

How to cite: *Angew. Chem. Int. Ed.* **2019**, *58*, 8917–8921
Angew. Chem. **2019**, *131*, 9010–9014

[1] a) E. Fabbri, A. Habereder, K. Waltar, R. Kötz, T. J. Schmidt, *Catal. Sci. Technol.* **2014**, *4*, 3800–3821; b) Q. Zhao, Z. Yan, C. Chen, J. Chen, *Chem. Rev.* **2017**, *117*, 10121–10211.
[2] a) N. Cheng, Q. Liu, J. Tian, Y. Xue, A. M. Asiri, H. Jiang, Y. He, X. Sun, *Chem. Commun.* **2015**, *51*, 1616–1619; b) J. Zhang, Z. Zhao, Z. Xia, L. Dai, *Nat. Nanotechnol.* **2015**, *10*, 444–452.
[3] a) M.-S. Balogun, W. Qiu, H. Yang, W. Fan, Y. Huang, P. Fang, G. Li, H. Ji, Y. Tong, *Energy Environ. Sci.* **2016**, *9*, 3411–3416; b) X. Lu, W.-L. Yim, B. H. Suryanto, C. Zhao, *J. Am. Chem. Soc.* **2015**, *137*, 2901–2907.
[4] a) H. B. Yang, J. Miao, S.-F. Hung, J. Chen, H. B. Tao, X. Wang, L. Zhang, R. Chen, J. Gao, H. M. Chen, L. Dai, B. Liu, *Sci. Adv.* **2016**, *2*, e1501122; b) C. Tang, H.-F. Wang, X. Chen, B.-Q. Li, T.-Z. Hou, B. Zhang, Q. Zhang, M.-M. Titirici, F. Wei, *Adv. Mater.* **2016**, *28*, 6845–6851.

[5] G. Wen, S. Wu, B. Li, C. Dai, D. S. Su, *Angew. Chem. Int. Ed.* **2015**, *54*, 4105 – 4109; *Angew. Chem.* **2015**, *127*, 4178 – 4182.
[6] a) X. Feng, W. Pisula, K. Müllen, *J. Am. Chem. Soc.* **2007**, *129*, 14116 – 14117; b) X. Feng, W. Pisula, K. Müllen, *Pure Appl. Chem.* **2009**, *81*, 2203 – 2224.
[7] a) H. Wu, C. Su, R. Tandiana, C. Liu, C. Qiu, Y. Bao, J. Wu, Y. Xu, J. Lu, D. Fan, K. P. Loh, *Angew. Chem. Int. Ed.* **2018**, *57*, 10848 – 10853; *Angew. Chem.* **2018**, *130*, 11014 – 11019; b) Y. Lin, K.-H. Wu, L. Yu, S. Heumann, D. S. Su, *ChemSusChem* **2017**, *10*, 3497 – 3505.
[8] a) P. Garrido-Barros, C. Gimbert-Suriñach, D. Moonshiram, A. Picón, P. Monge, V. S. Batista, A. Llobet, *J. Am. Chem. Soc.* **2017**, *139*, 12907 – 12910; b) H. Lei, C. Liu, Z. Wang, Z. Zhang, M. Zhang, X. Chang, W. Zhang, R. Cao, *ACS Catal.* **2016**, *6*, 6429 – 6437; c) F. Li, B. Zhang, X. Li, Y. Jiang, L. Chen, Y. Li, L. Sun, *Angew. Chem. Int. Ed.* **2011**, *50*, 12276 – 12279; *Angew. Chem.* **2011**, *123*, 12484 – 12487.
[9] Y. Lin, Z. Feng, L. Yu, Q. Gu, S. Wu, D. S. Su, *Chem. Commun.* **2017**, *53*, 4834 – 4837.
[10] X.-L. Wang, L.-Z. Dong, M. Qiao, Y.-J. Tang, J. Liu, Y. Li, S.-L. Li, J.-X. Su, Y.-Q. Lan, *Angew. Chem. Int. Ed.* **2018**, *57*, 9660 – 9664; *Angew. Chem.* **2018**, *130*, 9808 – 9812.
[11] a) C. Wang, H. Yang, Y. Zhang, Q. Wang, *Angew. Chem. Int. Ed.* **2019**, *58*, 1 – 6; *Angew. Chem.* **2019**, *131*, 1 – 1; b) M. Görlin, J. Ferreira de Araújo, H. Schmies, D. Bernsmeier, S. r. Dresp, M. Gliech, Z. Jusys, P. Chernev, R. Kraehnert, H. Dau, P. Strasser, *J. Am. Chem. Soc.* **2017**, *139*, 2070 – 2082.
[12] a) L. Zhang, J. Xiao, H. Wang, M. Shao, *ACS Catal.* **2017**, *7*, 7855 – 7865; b) W. Wang, J. Luo, S. Chen, *Chem. Commun.* **2017**, *53*, 11556 – 11559.
[13] E. C. M. Tse, T. T. H. Hoang, J. A. Varnell, A. A. Gewirth, *ACS Catal.* **2016**, *6*, 5706 – 5714.
[14] C. Yang, O. Fontaine, J.-M. Tarascon, A. Grimaud, *Angew. Chem. Int. Ed.* **2017**, *56*, 8652 – 8656; *Angew. Chem.* **2017**, *129*, 8778 – 8782.
[15] K. Sakaushi, A. Lyalin, T. Taketsugu, K. Uosaki, arXiv preprint arXiv:1801.01230, **2018**.
[16] T. Shinagawa, A. T. Garcia-Esparza, K. Takanabe, *Sci. Rep.* **2015**, *5*, 13801.

Manuscript received: March 7, 2019
Revised manuscript received: April 9, 2019
Accepted manuscript online: April 15, 2019
Version of record online: May 17, 2019

